Measurement of the $^{14}O(\alpha, p)^{17}F$ cross section at $E_{c.m.} \approx 2.1$–5.3 MeV

A. Kim,[1,*] N. H. Lee,[1] M. H. Han,[2] J. S. Yoo,[2] K. I. Hahn,[1,2,†] H. Yamaguchi,[3] D. N. Binh,[3] T. Hashimoto,[3] S. Hayakawa,[3] D. Kahl,[3] T. Kawabata,[3] Y. Kurihara,[3] Y. Wakabayashi,[3] S. Kubono,[4,5] S. Choi,[6] Y. K. Kwon,[7] J. Y. Moon,[7] H. S. Jung,[8] C. S. Lee,[8] T. Teranishi,[9] S. Kato,[10] T. Komatsubara,[11] B. Guo,[12] W. P. Liu,[12] B. Wang,[12] and Y. Wang[12]

[1]*Department of Physics, Ewha Womans University, Seoul 120-750, Korea*
[2]*Department of Science Education, Ewha Womans University, Seoul 120-750, Korea*
[3]*Center for Nuclear Study, University of Tokyo, RIKEN Branch, Japan*
[4]*RIKEN Nishina Center, Wako 351-0198, Japan*
[5]*Institute of Modern Physics, Lanzhou, China*
[6]*Department of Physics and Astronomy, Seoul National University, Seoul 151-742, Korea*
[7]*Institute for Basic Science, Daejeon 305-811, Korea*
[8]*Department of Physics, Chung-Ang University, Seoul 156-756, Korea*
[9]*Kyushu University, Fukuoka 812-8581, Japan*
[10]*Yamagata University, Yamagata 990-8560, Japan*
[11]*Tsukuba University, Ibaraki 305-8577, Japan*
[12]*China Institute of Atomic Energy, Beijing, China*

(Received 17 June 2015; published 1 September 2015)

Background: The $^{14}O(\alpha, p)^{17}F$ reaction plays an important role as the trigger reaction for the x-ray burst.
Purpose: The direct measurement of $^{14}O(\alpha, p)^{17}F$ was made for studying the resonant states in ^{18}Ne and determining the reaction rate of $^{14}O(\alpha, p)^{17}F$ at astrophysical temperatures.
Methods: The differential cross section of the $^{14}O(\alpha, p)^{17}F$ reaction was measured using a 2.5-MeV/u ^{14}O radioactive beam and the thick target method in inverse kinematics. Three sets of ΔE-E Si telescopes were installed and coincidence measurements were performed. We analyzed single-proton decay events using the time-of-flight (TOF) information of the recoiling protons.
Results: The excitation function of $^{14}O(\alpha, p)^{17}F$ was acquired for excitation energies between 7.2 and 10.4 MeV in ^{18}Ne by considering the two channels which decay to the ground state and first excited state of ^{17}F. Several new, as well as previously known, states in ^{18}Ne were observed and their resonance parameters were extracted from R-matrix analysis. The contributions of four resonances over the excitation energy range, $7 < E_x < 8.2$ MeV, to the $^{14}O(\alpha, p)^{17}F$ reaction rate were calculated.
Conclusions: We observed very strong single-proton decay events, but did not observe strong double-proton decay events as in a previous study by Fu *et al.* The reaction rates contributed by the 7.35-, 7.58-, and 7.72-MeV states were estimated to be dominant at temperatures $T_9 > 2$. Among these three states, the 7.35-MeV state was found to enhance the reaction rate by a factor of 10 greater than the other two resonance states.

DOI: 10.1103/PhysRevC.92.035801 PACS number(s): 25.55.−e, 26.30.−k, 27.20.+n

I. INTRODUCTION

The $^{14}O(\alpha, p)^{17}F$ reaction is known as the trigger reaction of an x-ray burst, which is a main source for producing the proton-rich nuclei through the rp-process. The α-induced reaction on ^{14}O can initiate the synthesis of heavy elements at temperatures higher than 10^9 K through the following αp-$p\gamma$ sequence: $^{14}O(\alpha, p)^{17}F(p, \gamma)^{18}Ne(\alpha, p)^{21}Na$ [1]. Thus the properties of the intermediate states in ^{18}Ne above the α threshold are important for understanding the reaction rate.

The excited states of ^{18}Ne have been studied using the time-reverse method or indirect methods by other groups [2–6]. The first direct measurement of the $^{14}O(\alpha, p)^{17}F$ reaction using the thick target method was reported in Ref. [5]. However, their results are ambiguous because of unclear identification of protons from many different channels. A more recent direct measurement by Ref. [6] reported that double-proton decays of the sequence $^{18}Ne^* \rightarrow {}^{17}F^* + p \rightarrow {}^{16}O + p + p$ were dominant in the high energy region ($E_x > 8$ MeV).

In the present study, the $^{14}O(\alpha, p)^{17}F$ reaction was measured directly in the energy range $E_{c.m.} = 2.1$–5.3 MeV, which corresponds to $E_x = 7.2$–10.4 MeV in ^{18}Ne. Although the crucial resonance arises from the $J^\pi = 1^-$ state at 6.15 MeV in ^{18}Ne, several excited states above 7 MeV of ^{18}Ne may also significantly contribute to the reaction rate at extremely high temperatures (3×10^9 K) [3]. The excitation function of $^{14}O(\alpha, p)^{17}F$ was obtained by analyzing protons decaying to ^{17}F.

II. EXPERIMENT

The direct measurement of the $^{14}O(\alpha, p)^{17}F$ reaction was performed using the thick target method in inverse

*Present address: Department of Physics, Sung Kyun Kwan University, Suwon 440-746, Korea.
†ishahn@ewha.ac.kr

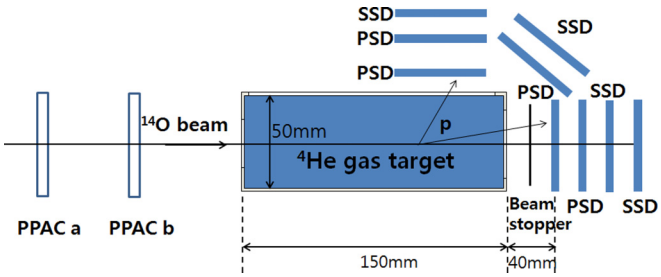

FIG. 1. (Color online) Schematic view of the experimental setup.

kinematics, which can provide a continuous excitation function. A radioactive ^{14}O beam was produced by the (p,n) reaction in a H_2 gas target bombarded by the primary ^{14}N beam of 8.4 MeV/u. The primary beam was transported from the azimuthally-varying-field (AVF) cyclotron of the Radioisotope (RI) Beam Factory of RIKEN Nishina Center to the low-energy RI beam separator, CRIB of the Center for Nuclear Study, University of Tokyo [7]. The maximum primary beam intensity was 170 pnA and the H_2 gas cell was cooled to 90 K by liquid nitrogen in order to improve the intensity of the ^{14}O beam [8].

A schematic view of the experimental setup is shown in Fig. 1. Two parallel plate avalanche counters (PPACs) [9] were installed in the F3 chamber before the helium gas target, where the (α,p) reaction occurred. These counters were used to identify a radioactive ^{14}O beam by measuring the time of flights (TOFs). Figure 2 shows the particle identification for a radioactive ^{14}O beam and contaminants. The main contamination of the secondary beams was ^{11}C and ^{14}N. The ^{14}O beam was selectively purified by a Wien filter system so that the beam purity was 90% at the experimental focal plane (F3) of CRIB. The ^{14}O beam intensity was about 5×10^5/s. The length of the ^{4}He gas target cell was 150 mm and the gas pressure was 440 torr at room temperature. This is equivalent to the effective thickness of 1.43 mg/cm^2. The entrance, exit, and side windows of the target cell were made

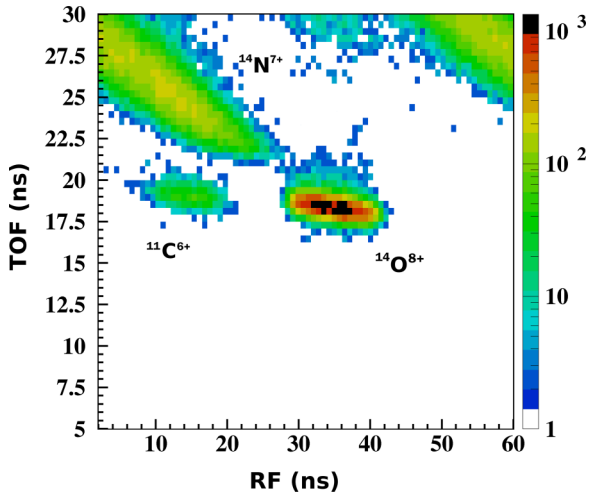

FIG. 2. (Color online) Secondary beam identification. The y axis and x axis represent TOFs between two PPACs and RF time (the timing between F0 and F3), respectively.

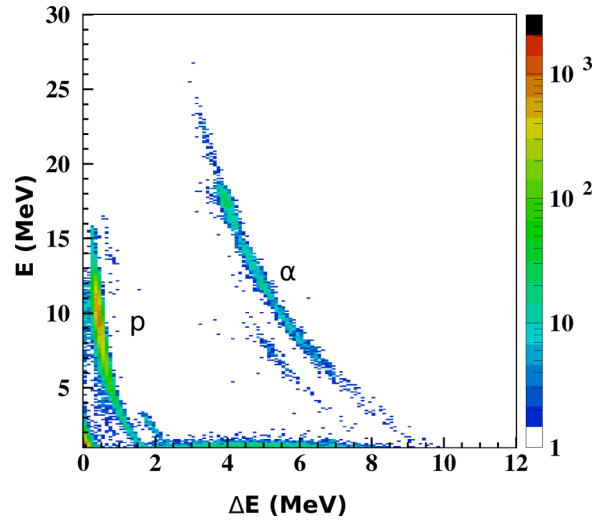

FIG. 3. (Color online) Particle identification in ΔE-E telescope.

of 2.5-μm-thick Havar foil. A 12-μm-thick aluminum foil was installed before the central telescope for stopping the beam. The final radioactive ^{14}O beam energy was 33.8 ± 0.5 MeV before the entrance window of the gas target, and this beam energy allowed an investigation of ^{18}Ne levels for E_x = 7.2–10.4 MeV ($E_{\text{c.m.}}$ = 2.1–5.3 MeV).

The recoiling protons were detected using three sets of ΔE-E telescopes consisting of position sensitive silicon detectors (PSDs) for ΔE and single strip silicon detectors (SSDs) for E as shown in Fig. 1. The three telescopes, consisting of one central telescope and two side telescopes, covered a laboratory angular range from -12° to 78° for events that occurred at the middle of the gas target. The central telescope consisted of 20-μm-, 73-μm-, 1.5-mm-, and 1.5-mm-thick silicon detectors. The thinnest (20-μm) detector was used for ΔE measurement. The closest PSD to the side window was 65 μm thick. The thicknesses of the PSDs and SSDs in the two side telescopes were 480 μm and 1.5 mm, respectively. The area of each silicon detector was 4.8×4.8 cm^2. If the ^{14}O$(\alpha,p)^{17}$F reaction occurs at the middle of the target, the beam energy $E_{\text{c.m.}}$ is 3.7 MeV and the central telescope can detect protons between the c.m. angles of 146° and 171°. For energy calibration, the proton beams of 10, 15, and 20 MeV as well as a mixed α source (E_α = 4.788, 5.486, and 5.805 MeV from ^{237}Np, ^{241}Am, and ^{244}Cm, respectively) were used.

III. ANALYSIS

Figure 3 shows the ΔE-E information of various recoiling particles. Protons from the (α,p) reaction were clearly identified. Protons may originate from either the single-proton decays (^{18}Ne$^* \rightarrow {}^{17}$F $+ p$) or double-proton decays (^{18}Ne$^* \rightarrow {}^{17}$F$^* + p \rightarrow {}^{16}$O $+ 2p$ or ^{18}Ne$^* \rightarrow {}^{16}$O $+ 2p$) [6,10–13].

In the analysis, the multiplicity of silicon detectors was investigated. We made an analysis on events where there were two protons detected in coincidence. There are two mechanisms to produce double protons from the ^{14}O $+ \alpha$

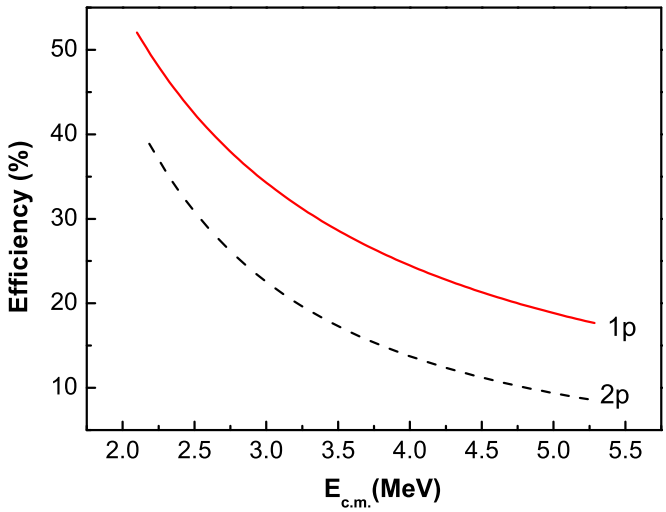

FIG. 4. (Color online) Geometrical efficiency which the present detector system detects two protons simultaneously (dotted line) and the efficiency for detecting the single proton (solid line).

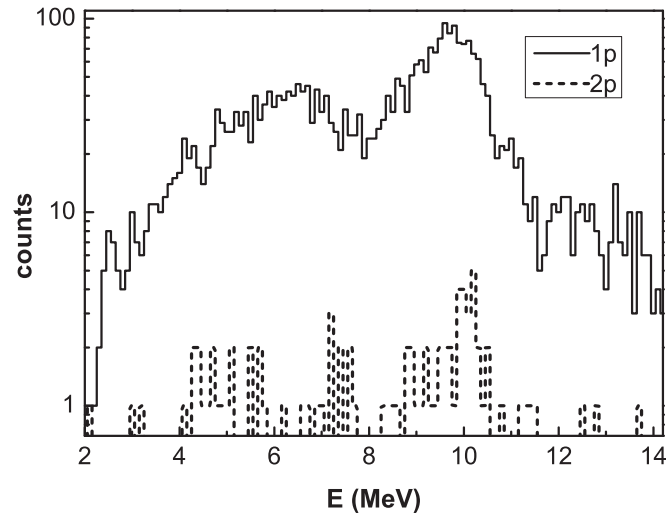

FIG. 5. Energy distribution of single- and double-proton events. The x axis represents the energy summation of the ΔE-E detector.

reaction. One is the democratic decay event, which decays directly to ^{16}O and $2p$ without forming excited states of ^{17}F. The other is the sequential decay event, which decays to $^{16}O + 2p$ through $^{17}F^*$. According to Ref. [12], the democratic decay and the sequential decay have similar relative momentum and angular distribution between two protons, but the number of events of the democratic decay is about 50% larger than that of the sequential decay. For the estimation of geometrical efficiency, we considered all the processes as democratic, i.e., we assumed that all protons come from a double-proton decay process and that ^{18}Ne decays into three particles (^{16}O and $2p$) isotropically in the c.m. frame. As a result, the geometrical efficiency for detecting two protons from the double-proton decay was estimated to be 15% and the solid angle was about 1.0 sr at the center of the target as shown in Fig. 4. The solid angle inferred from the experimental geometry in Ref. [6] was about 1.2 sr, which is very similar to our case. If the double-proton decay events are very common as reported in Ref. [6], our estimated detection efficiency would be sufficient to reconstruct the process of $^{18}Ne^*(\rightarrow {}^{17}F^* + p) \rightarrow {}^{16}O + 2p$.

Figure 5 shows the energy distribution of $1p$ and $2p$ decays. As represented in this figure, our data show that the ratio of $2p$ to $1p$ is less than 0.03, which indicates the double-proton decay channel is very rare. In the case of a double-proton decay, a recent experiment [13] also reported that the $2p$ decay channel was not observed in $E_x = 5.1$–8.1 MeV with the exception of decays from the 6.15-MeV state where $2p/1p \leqslant 0.27$. Because the statistics of $2p$ events are too small to reconstruct the proton spectra, they were excluded from our analysis but are considered in the error estimation.

Single-proton decay can proceed to the ground state of ^{17}F or it can go to one of the excited states of $^{17}F^*$, i.e., $^{14}O(\alpha,p)^{17}F_{g.s.}$ or $^{14}O(\alpha,p)^{17}F^*$. As shown in Fig. 6, protons decaying from high lying states (>7 MeV) of ^{18}Ne to the ground state of ^{17}F as well as one of the three excited states of ^{17}F could be observed in our energy range. However, the energy difference between the ground state and the first excited state of ^{17}F is only 0.5 MeV, and the discrimination between p_0 and p_1 protons (decays to the ground and first excited state, respectively) is not possible due to the experimental time resolution. The energy difference between the first and second excited states of ^{17}F is more than 2 MeV, so that protons from higher excited states, p_2 and p_3, can be separated by the TOF information between the PPAC and the Si detector. Figure 7 shows the TOF-energy plots acquired from the experimental data and a simulation for the detector at zero degrees. While the boundary between the p_0-p_1 events and the p_2-p_3 events is not clear in the region of $E_p < 8$ MeV, the p_0-p_1 group could be identified clearly for $E_p > 8$ MeV consistent with the simulation. The time resolution was 2 ns and the broad time distribution was due to the energy spread in the He gas target which made discrimination of p_0-p_1 difficult in the low energy region. The ratio p_2-p_3/p_0-p_1 was 0.51 and only the p_0-p_1 group was used for acquiring the excitation function in this study. Figure 8 shows the proton energy spectra of p_2-p_3. Because the p_2 and p_3 events are also indistinguishable, the solid and dotted lines represent when all the events in the p_2-p_3

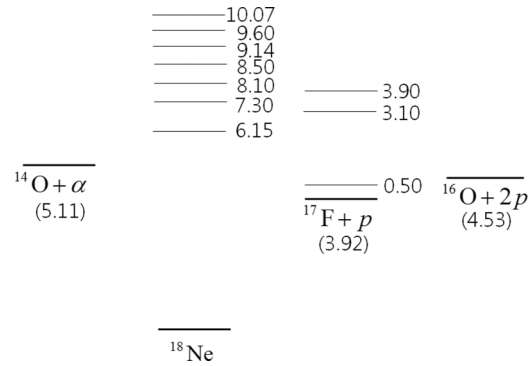

FIG. 6. Threshold energy of p decay, $2p$ decay, and α and the energy level of ^{18}Ne. Several excited levels are also shown with the excitation energies.

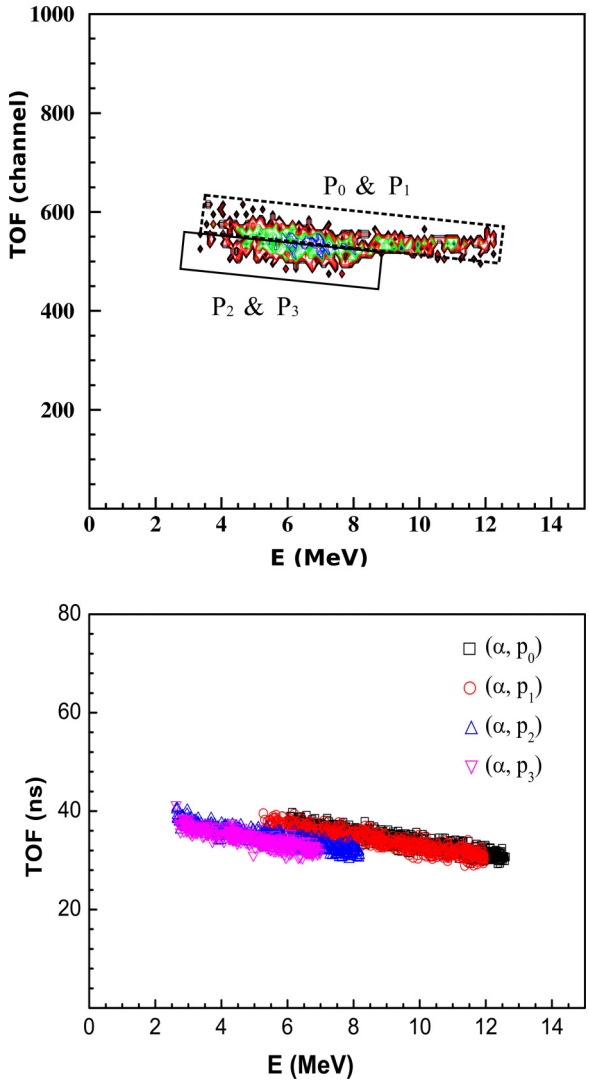

FIG. 7. (Color online) TOF between the PPAC and the central telescope plotted against the energy of protons. The upper panel represents the experimental data and the lower panel shows the simulation results at zero degrees.

group go to the second and third states of ^{17}F, respectively. It was concluded that these events did not contribute to the spectra of $E_{\text{c.m.}} < 3.3$ MeV due to the kinematics condition.

For the reconstruction of p_0-p_1, it was assumed that p_0 is dominant based on the results by Almaraz-Calderon *et al.* and Bardayan *et al.* [13,14]. Although the energy ranges reported in Refs. [13,14] are not exactly the same, they partially overlap with this work between 7 and 8 MeV in E_x. There is no available information on the decay widths Γ_{p_1} in higher lying states. In Fig. 7, the p_0 and p_1 energy ranges seem to be extended down to 4 MeV while the one of simulation is cut off at about 5 MeV. This low energy part was excluded after the kinematics calculation because this might be from background proton sources such as the plastic films used at upstream detectors.

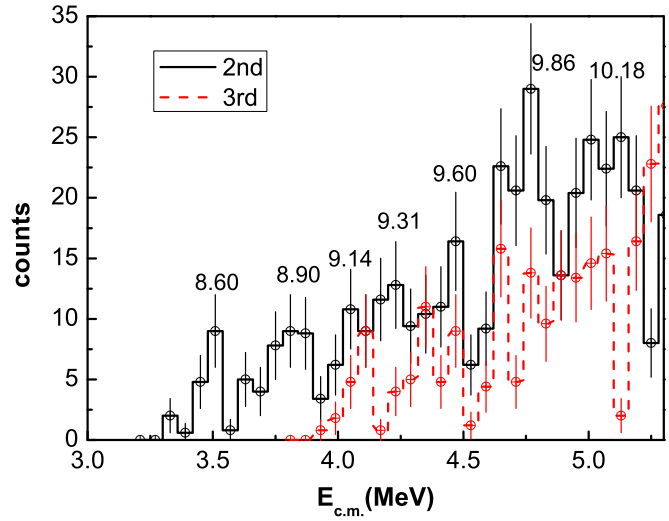

FIG. 8. (Color online) Proton spectra of p_2-p_3, when all the protons go to the second state (solid line) and third state (dotted line) of ^{17}F.

IV. DISCUSSION AND RESULTS

The reconstructed proton spectrum was fitted with the R-matrix [15] analysis (SAMMY 8.0 [16]). R-matrix fitting was performed by dividing the spectrum into two energy regions, $7 < E_x < 8.2$ MeV and 8.2 MeV $< E_x$, due to the relatively small statistics at the low energy region and the difference in the angular acceptance between the two energy regions from the thick target method. The 8.10-MeV state was included in both energy regions in our R-matrix calculations. The channel radius was given by $1.4(A_{^{14}\text{O}}^{1/3} + A_{^{4}\text{He}}^{1/3})$ fm. Because ^{14}O and ^{4}He in the entrance channel are spinless, only natural parity states were considered.

A. States in $7 < E_x < 8.2$ MeV

Six resonances at $E_x = 7.05$, 7.35, 7.60, 7.72, 7.95, and 8.09 MeV were identified previously in Refs. [2,3,13,17–19]. In this study, four resonances at $E_x = 7.35$, 7.58, 7.72, and 8.10 MeV were observed and their extracted resonant parameters were summarized in Table I. Because the 7.05-MeV state is out of the experimental energy range, it was not observed. Figure 9 shows the differential cross section for $^{14}\text{O}(\alpha, p_0)^{17}\text{F}$ at $E_x < 8.2$ MeV and R-matrix fitted curves. After fixing the J^π value of the 8.10 MeV state to be 0^+, because the 0^+ assignment gave the best χ^2 for both the $E_x < 8.2$ and $E_x > 8.2$ MeV regions, 10 different combinations for assigning spins and parities for other peaks were considered and their χ^2 values were obtained.

The 7.35-MeV state was difficult to be identified due to very low statistics and featureless structure in our data, but fitted results of the other two resonances relied much on its existence and spin-parity. When the J^π was assigned with 1^- instead of 2^+ as shown in the top and bottom of Fig. 9, fitted curves had a factor of 1.7 smaller χ^2 value. He *et al.* assigned $J^\pi = 2^+$, while Hahn *et al.* considered 1^- at $E_x = 7.35$ MeV based on the mirror state. Harss *et al.* assigned 1^- or 4^+ at $E_x = 7.37$ MeV by comparing the widths of mirror states in

TABLE I. Resonant parameters of states in ^{18}Ne with $7 < E_x < 8.2$ MeV.

E_x (MeV)	$E_{c.m.}$(MeV)	Γ_α (keV)	Γ_p (keV)	J^π	$\omega\gamma$ (keV)
7.35 ± 0.03	2.25	3.1 ± 0.2	387.0 ± 40.0	(1^-)	9.32
7.58 ± 0.02	2.46	1.5 ± 0.5	102.0 ± 26.0	(0^+)	1.52
7.72 ± 0.02	2.61	1.9 ± 0.3	279.0 ± 61.0	$(2^+,3^-)$	5.38
8.10 ± 0.10	2.99	40.4 ± 4.9	298.0 ± 38.0	(0^+)	35.0

Ref. [19]. However, a few years later, Harss *et al.* proposed 2^+ by adopting the argument on Coulomb shift of Fortune and Sherr [3,20]. In the present work, 1^- is more favorable based on the R-matrix calculation.

The 7.58-MeV state seems to correspond with the resonance at $E_x = 7.60$ or 7.62 MeV reported in Refs. [3,17,18] due to similar excitation energy within error. Harss *et al.* suggested 1^- due to its strong population through the (p,α) reaction. They expected this resonance to be 1^-, because the analog state of ^{18}O at $E_x = 7.616$ MeV has 1^-. Our data show that 0^+ could be chosen for the best fitting. There are some debates on the missing 0^+ state around this energy region in ^{18}O. A new state at $E_x = 7.796$ MeV as the band head of the $K^\pi = 0_4^+$ band was observed in Ref. [21], which was questioned in Ref. [22]. Fortune and Sherr insisted that if the 7.796-MeV state in ^{18}O is the missing 6-particle–4-hole (6p-4h) state with 0^+, this cannot be the mirror state of the 7.37-MeV state in ^{18}Ne because the energy shift is much larger than their calculated value and the parity is opposite. Therefore, if the 7.796-MeV state newly observed in Ref. [21] has $J^\pi = 0^+$, there should be a corresponding mirror state in ^{18}Ne. The 7.58-MeV state assigned with 0^+ in this study could be a candidate for the mirror state of the 7.796-MeV state in ^{18}O.

Because the 7.72-MeV state was not observed through $^{17}F(p,\alpha)^{14}O$ in Ref. [3], Harss *et al.* assigned it the unnatural parity, 2^-. In the present (α,p) measurement, the 7.72-MeV state was clearly observed. We considered two natural parities, 2^+ and 3^-, which produce the least χ^2 values as shown in the lower panel of Fig. 9. Even though the assignment of $J^\pi = 2^+$ has a smaller χ^2 value, 3^- also seems to be matched with the data in the region of $E_{c.m.} < 2.8$ MeV. The combination of 1^--0^+-3^- gives the χ^2 value of 0.83, which is considerably smaller than other combinations.

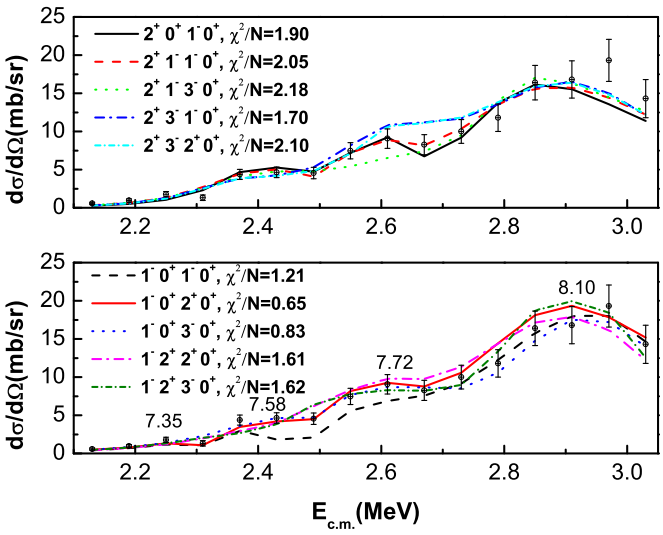

FIG. 9. (Color online) Fitted curves of excitation function of $^{14}O(\alpha,p)^{17}F_{g.s.}$ with 10 different J^π combinations in $7 < E_x < 8.2$ MeV. The resonance at $E_x = 8.10$ MeV was fixed with 0^+. The solid line in the bottom figure represents the best fitted curve.

The 8.10-MeV resonance corresponds to a previously observed state at 8.10 MeV in Ref. [2], 8.09 MeV in Ref. [13], and 8.11-MeV in Ref. [18]. This level was assigned as $J^\pi = 5^-$ by a theoretical study in Ref. [25]. Almaraz-Calderon *et al.* and Hu *et al.* assigned 3^- using experimental data from the $^{16}O(^3He,n)^{17}Ne$ reaction and the $^{17}F(p,p)^{17}F$ reaction, respectively. However, in this study, our data fit much better with $J^\pi = 0^+$ than $J^\pi = 5^-$ or 3^-.

B. Astrophysical implication

The $^{14}O(\alpha,p)^{17}F$ reaction rate contributed by three resonances observed in this study could be evaluated with the resonance parameters listed in Table I. The reaction rate through isolated and narrow resonances is given by

$$N_A\langle\sigma v\rangle = 1.54 \times 10^{11}(AT_9)^{(-3/2)} \times \omega\gamma \times \exp\left(-11.605\frac{E_r}{T_9}\right), \quad (1)$$

where N_A is Avogadro's number, A is the reduced mass, T_9 is the temperature, and E_r is the resonance energy. The estimated reaction rate is presented in Fig. 10. Because only the (α,p_0) channel was considered, $\Gamma_{tot} = \Gamma_\alpha + \Gamma_p$ was used as the total width. The $^{14}O(\alpha,p)^{17}F$ reaction rate is known for being dominated by the 1^- state at $E_x = 6.15$ MeV. As shown in Fig. 10, the contribution of the 1^- state at 6.15 MeV is a factor of 100 larger than the other three resonances in the $0.5 < T_9 < 1.5$ region. However, as the temperature increases to more than $T_9 = 1.5$, the higher energy resonances become important. In particular, the contribution by the 1^- 7.35-MeV state begins to surpass the contribution by the 1^- 6.15-MeV state in the region of $T_9 > 2$. As a result, the three resonances in $E_x = 7$–8 MeV dominate the reaction rate at extremely high temperature ($T_9 > 2$). For the 7.05-MeV state, which was observed in previous studies, it gives similar contribution to the 7.35-MeV state in the region of $T_9 < 1$. However, when the temperature is higher than 2 GK, its impact on the reaction rate is found to be smaller than the other resonances observed in this study. The $^{14}O(\alpha,p)^{17}F$ rate with the 8.10-MeV resonance contribution was calculated in Ref. [13], which shows that it plays an important role in the reaction rate at $T_9 > 3$. The resonance strength $\omega\gamma$ deduced in Ref. [13] is about 35 keV,

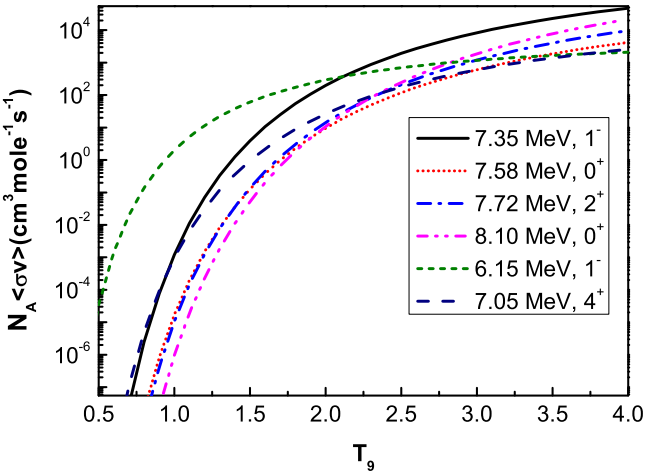

FIG. 10. (Color online) Reaction rates contributed by four resonances observed in this study, 6.15- and 7.05-MeV states. The resonant parameters of 6.15- and 7.05-MeV states were adopted from Refs. [23] and [3], respectively.

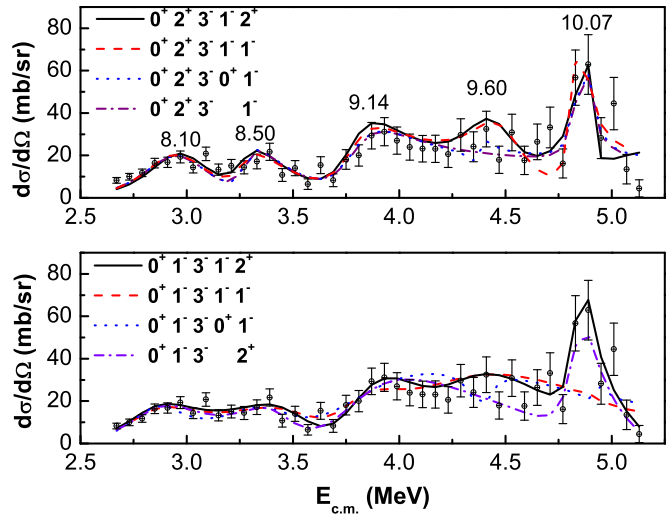

FIG. 11. (Color online) Excitation function of ^{14}O$(\alpha, p_0)^{17}$F$_{g.s.}$ with eight different J^π assignments in $E_x > 8$ MeV. The solid line in the bottom figure represents the best fitted curve.

which is almost the same as our data. This is because $\frac{\Gamma_\alpha \Gamma_p}{\Gamma_{tot}}$ of our data is 7 times larger than the one of Ref. [13], while $2J + 1$ in case of 0^+ assignment is 7 times smaller than the one of 3^-. Therefore, there is almost no difference in estimating the final reaction rate contribution by the 8.10-MeV state.

C. States in $E_x > 8.2$ MeV

The four resonances at 8.50, 9.14, 9.60, and 10.07 MeV were analyzed with the fitting parameters listed in Table II and the resonance at 8.10 MeV was included in the fitting. J^π values of these resonances were adopted from their mirror states in the ^{18}O nucleus as reported in Ref. [24]. However, their J^π assignments were not the same as the ^{18}O levels and several J^π combinations were used in the R-matrix calculation. Among the five resonances, two most critical J^π assignments were 0^+ at 8.10 MeV and 3^- at 9.14 MeV, since any other J^π values for these two resonances produce significant deviation from the experimental data. Therefore, we fixed the 0^+ and 3^- states, while we searched J^π assignments among 0^+, 1^-, and 2^+ for the other three resonances. The assignment of 0^+ at 8.10 MeV was consistent with the data analysis of $E_x < 8.3$ MeV. Figure 11 shows the results of the R matrix. The top and bottom spectra in Fig. 11 represent $J^\pi = 2^+$ and 1^-, respectively, for the $E_x = 8.50$-MeV state ($E_{c.m.} = 3.39$ MeV). The best fitted curve is from the combination of 0^+-1^--3^--1^--2^+ as shown in the bottom spectrum, which has the least χ^2 value. However, these J^π assignments are still not conclusive because the curves of the other seven combinations are also consistent with the measurement, since their χ^2 are slightly higher than the combination of 0^+-1^--3^--1^--2^+. The 8.50- and 9.14-MeV resonances were observed in our previous results of ^{14}O + α elastic scattering [26] as well as in Ref. [27].

The resonance at 8.50 MeV was identified first via the ^{16}O(^{3}He,n)^{18}Ne reaction [28], but its spin-parity was not assigned. In this study, the assignment of 1^- is suggested as the best candidate based on the R-matrix analysis. Comparing the mirror nucleus, ^{18}O, several 1^- states were reported around 9 MeV while the 2^+ state was not observed. However, the fitted curve with 2^+, which makes the peak sharper as shown in Fig. 11, also gives a similar χ^2 value. We tentatively suggest both 1^- and 2^+ as possible assignments for this resonance.

There is a strong resonance at $E_x = 9.14$ MeV, which agrees within errors with the resonance at $E_x = 9.20$ MeV as reported in Refs. [29,30], measured via the ^{20}Ne$(p,t)^{18}$Ne reaction. The spin and parity were not assigned in the previous (p,t) reaction. Our analysis shows that $J^\pi = 3^-$ fits our data the best and is consistent with recent studies using the α elastic scattering on ^{14}O [6,26]. In addition, the observation of strong 3^- at 9.36 MeV in ^{18}O supports its J^π assignments [24,35].

TABLE II. R-matrix fit parameters and the results of shell model calculations in $E_x > 8.2$ MeV.

E_x (MeV)	$E_{c.m.}$ (MeV)	Γ_α (keV)	Γ_p (keV)	J^π	E_x^{SM}	J^π(SM)
8.50 ± 0.10	3.39	84.5 ± 21.0	546.0 ± 60.0	$(1^-, 2^+)$		
9.14 ± 0.10	4.03	27.0 ± 6.0	467.5 ± 59.0	3^-	9.47	3^-
					(9.27	4^+)
9.60 ± 0.09	4.49	620.0 ± 104.0	7.8 ± 6.6	$(1^-, 0^+)$	10.02	1^-
10.07 ± 0.08	4.96	1.5 ± 0.8	90.0 ± 18.0	$(2^+, 1^-)$	10.06	2^+
					(10.10	0^+)

We observed two new resonances at $E_x = 9.60$ and $E_x = 10.07$ MeV. We also performed shell model calculations to study excitation energies with their spins and parities. The calculations were carried out in the *spsdpf* model space with the WBB interaction [31] using the code NUSHELL@MSU [32]. Only five resonances which have natural parities were obtained within the energy range of $7.5 < E_x < 10.5$ MeV from shell model calculations and their results are listed in Table II. Calculated J^π values for the states $E_x > 9$ MeV are consistent with our results except for the 4^+ resonance (d wave) expected at 9.27 MeV. The resonance of 4^+ was observed at $E_x = 10.29$ and 10.26 MeV in ^{18}O [33,35], but in case of ^{18}Ne, no 4^+ resonance was reported at the high energy region.

The spin-parity for the resonance at 9.60 MeV was not unique with our data. Our analysis indicates its assignment to be 1^-, however, another possibility such as 0^+ cannot be ruled out. This may be a superposition of two or more resonances. If J^π of 1^- is confirmed, the 9.60-MeV state ($\Gamma_\alpha \sim 620$ keV) could be the analog state of a very broad 1^- resonance of the mirror nuclei [34,35]. The $E_x = 9.8$ MeV state of ^{18}O was measured in Ref. [34] using β-delayed α spectrum of ^{18}N. It has an α width of 560 keV. The $E_x = 10.46$ MeV state of ^{18}O has a total width of 800 keV as obtained in a study of the α cluster structure of ^{18}O [35].

The measurement of the $^{14}O(\alpha,p)^{17}F$ reaction is essential for studying the synthesis of heavy nuclei up to Cd and the source of energy generation in an x-ray burst. Our study shows that the resonances in $7 < E_x < 8.2$ MeV might be astrophysically important in the region of $T_9 > 2$. In particular, the contribution by the 1^- state at $E_x = 7.35$ MeV was about a factor of 10 larger than the other two resonances at $E_x = 7.58$ and 7.72 MeV in the entire temperature.

V. CONCLUSIONS

The $^{14}O(\alpha,p)^{17}F$ reaction was measured directly using a radioactive ^{14}O beam for studying the resonance properties of ^{18}Ne. The results show that in the energy range $E_x \sim 7.2$–10.4 MeV, the single-proton decay mode is dominant when compared to the double-proton decay mode of ^{18}Ne. The newly observed 9.60- and 10.07-MeV states as well as previously known 7.35-, 7.58-, 7.72-, 8.10-, 8.50-, and 9.14-MeV states were analyzed and their resonance parameters were extracted from R-matrix calculations. These are the first results for identifying the resonant states in a wide energy region, $7 < E_x < 10$ MeV through the direct measurement of the $^{14}O(\alpha,p)^{17}F$ reaction. In addition, the reaction rate contributed by the 7.35-, 7.58-, and 7.72-MeV states is estimated to be dominant in $T_9 > 2$. However, because it was not possible to distinguish protons decaying to the first excited state from protons decaying to the ground state of ^{17}F, more studies with better detector techniques, which allow us to experimentally determine the reaction points in the target, are desirable.

ACKNOWLEDGMENTS

The authors thank RIKEN and CNS staffs for their operation of the AVF cyclotron. This work was supported by the Basic Science Research Program through the National Research Foundation of Korea (NRF) grant funded by the Ministry of Education (Grants No. NRF-2010-0027136, No. NRF-2012R1A1A3007962, and No. NRF-2014R1A1A2A16052632) and by JSPS KAKENHI (Grants No. 21340053 and No. 25800125). C.S.L. was supported by the National Research Foundation grant funded by the Korean Government (Grants No. NRF-2009-0093817 and No. NRF-2013R1A1A2063017).

[1] R. K. Wallace and S. E. Woosley, Astrophys. J. Suppl. Ser. **45**, 389 (1981).
[2] K. I. Hahn *et al.*, Phys. Rev. C **54**, 1999 (1996).
[3] B. Harss *et al.*, Phys. Rev. C **65**, 035803 (2002).
[4] J. C. Blackmon *et al.*, Nucl. Phys. A **718**, 127 (2003).
[5] M. Notani *et al.*, Nucl. Phys. A **746**, 113c (2004).
[6] C. Fu *et al.*, Phys. Rev. C **76**, 021603(R) (2007).
[7] Y. Yanagisawa *et al.*, Nucl. Instrum. Methods Phys. Res. Sect. A **539**, 74 (2005).
[8] H. Yamaguchi *et al.*, Nucl. Instrum. Methods Phys. Res. Sect. A **589**, 150 (2008).
[9] H. Kumagai *et al.*, Nucl. Instrum. Methods Phys. Res. Sect. A **470**, 562 (2001).
[10] J. Gomez del Campo *et al.*, Phys. Rev. Lett. **86**, 43 (2001).
[11] L. V. Grigorenko, R. C. Johnson, I. J. Thompson, and M. V. Zhukov, Phys. Rev. C **65**, 044612 (2002).
[12] G. Raciti, G. Cardella, M. De Napoli, E. Rapisarda, F. Amorini, and C. Sfienti, Phys. Rev. Lett. **100**, 192503 (2008).
[13] S. Almaraz-Calderon *et al.*, Phys. Rev. C **86**, 025801 (2012).
[14] D. Bardayan *et al.*, Phys. Rev. C **81**, 065802 (2010).
[15] A. M. Lane and R. G. Thomas, Rev. Mod. Phys. **30**, 257 (1958).
[16] N. M. Larson, ORNL/TM-9179/R5, 2000 (unpublished).
[17] J. J. He *et al.*, Eur. Phys. J. A **47**, 67 (2011).
[18] J. Hu *et al.*, Phys. Rev. C **90**, 025803 (2014).
[19] B. Harss *et al.*, Phys. Rev. Lett. **82**, 3964 (1999).
[20] H. T. Fortune and R. Sherr, Phys. Rev. Lett. **84**, 1635 (2000).
[21] W. von Oertzen *et al.*, Eur. Phys. J. A **43**, 17 (2010).
[22] H. T. Fortune and R. Sherr, Phys. Rev. C **84**, 047301 (2011).
[23] D. W. Bardayan, J. C. Blackmon, R. L. Kozub, M. Matos, and M. S. Smith, Phys. Rev. C **85**, 065805 (2012).
[24] E. D. Johnson *et al.*, Eur. Phys. J. A **42**, 135 (2009).
[25] M. Wiescher *et al.*, Astrophys. J. **316**, 162 (1987).
[26] A. Kim *et al.*, J. Kor. Phys. Soc. **57**, 40 (2010).
[27] C. Fu *et al.*, Phys. Rev. C **77**, 064314 (2008).
[28] A. V. Nero, E. G. Adelberger, and F. S. Dietrich, Phys. Rev. C **24**, 1864 (1981).
[29] W. R. Falk *et al.*, Nucl. Phys. A **157**, 241 (1970).
[30] R. A. Paddock, Phys. Rev. C **5**, 485 (1972).
[31] E. K. Warburton and B. A. Brown, Phys. Rev. C **46**, 923 (1992).
[32] B. A. Brown and W. D. Rae, MSU-NCSL Report, 2007 (unpublished).
[33] M. E. Cobern, L. C. Bland, H. T. Fortune, G. E. Moore, S. Mordechai, and R. Middleton, Phys. Rev. C **23**, 2387 (1981).
[34] L. Buchmann *et al.*, Phys. Rev. C **75**, 012804 (2007).
[35] V. Z. Goldberg *et al.*, Phys. At. Nucl. **68**, 1079 (2005).